Journal of Applied Physics

RESEARCH ARTICLE | APRIL 15 2025

Acoustic Su–Schrieffer–Heeger chain with phase nonreciprocal couplings

Tong Guo ; Liyun Cao ; Badreddine Assouar ; Brice Vincent ; Aurélien Merkel

J. Appl. Phys. 137, 153101 (2025)
https://doi.org/10.1063/5.0254537

Journal of Applied Physics ARTICLE pubs.aip.org/aip/jap

Acoustic Su–Schrieffer–Heeger chain with phase nonreciprocal couplings

Cite as: J. Appl. Phys. **137**, 153101 (2025); doi: 10.1063/5.0254537
Submitted: 23 December 2024 · Accepted: 26 March 2025 ·
Published Online: 15 April 2025

Tong Guo, Liyun Cao, Badreddine Assouar,[a] Brice Vincent, and Aurélien Merkel[b]

AFFILIATIONS

Université de Lorraine, CNRS, IJL, F-54000 Nancy, France

[a]**Electronic mail:** badreddine.assouar@univ-lorraine.fr
[b]**Author to whom correspondence should be addressed:** aurelien.merkel@univ-lorraine.fr

ABSTRACT

The Su–Schrieffer–Heeger model becomes non-Hermitian in general when the reciprocity of wave propagation is broken in the couplings. Here, we introduce phase non-reciprocity in the coupling of an acoustic Su–Schrieffer–Heeger chain by adding direction-dependent imaginary parts in the coupling strengths while keeping the real parts independent on the direction. We theoretically and numerically investigate the effect of the phase non-reciprocity on the band structure and the topology of the chain. The hermiticity is broken in general, but there is still one special case where the model remains Hermitian. An acoustic analog of this case is build where fluid flow is introduced in the couplings. In the non-Hermitian cases, the skin effect is visible except for one specific transition case where the system remains non-Hermitian but where reciprocity is maintained.

I. INTRODUCTION

The Su–Schrieffer–Heeger (SSH) model constitutes one of the seminal models for understanding the fundamentals of topological insulators. The unit cell of this one-dimensional crystal is composed of two sites that are coupled by intracell and intercell hoppings. The topological phases of an SSH chain are triggered by the dimerization induced by the couplings. By varying the relative real amplitudes of the couplings, one can travel from a trivial phase to a topological non-trivial phase passing through a topological phase transition when the amplitude of the couplings are equal. The effect of the topological non-trivial phase manifests itself when a finite chain is considered and where edge states are visible at the boundaries. The existence of these edge states is connected to the bulk via the Bulk Boundary Correspondence (BBC), which is one central concept of topology.

As extensively studied in the Hermitian case, the SSH model is also largely used to explore the topology of non-Hermitian systems. Non-hermiticity might break the conventional BBC because of the non-Hermitian skin effect where all the bulk states are localized at one boundary of the chain and, as a consequence, the edge states become undistinguishable and the topological invariant needs to be redefined.[1–3] The BBC can be re-established in non-Hermitian systems using the non-Bloch in a generalized Brillouin zone or the biorthogonal approaches.[4–8]

Non-hermiticity can be introduced in two different ways in the SSH model. In the first one, imaginary parts are added to the onsite potentials representing either gain or loss following the sign of the imaginary part. The topological properties of the Hermitian SSH chain are maintained with non-Hermitian parity-time symmetric onsite potentials.[9–14] The non-Hermitian potentials are then perturbations to the Hermitian system, and intriguing phenomena, such as a non-Hermitian higher-order state[15] and topological lasing,[16] have been observed. However, non-Hermitian onsite potentials taken alone can trigger the topological phase transition.[17–27] In this case, the required dimerization to trigger the topological phase transitions comes from the non-Hermitian potentials.[18,20,23,25,27]

The second way to introduce non-hermiticity is to consider non-reciprocal couplings between each site. In this case, the band structures with periodic boundary conditions can be drastically different from those with open boundary conditions, thus breaking the conventional BBC.[1–3] This is attributed to the non-Hermitian skin effect. The non-Hermitian skin effect has been extensively studied[28,29] and is in stark contrast to the Hermitian wave physics. It has been experimentally observed in mechanics,[30,31] optics,[32]

acoustics,[33–36] and electronic circuits.[37,38] The non-Hermitian skin effect can reshape the spatial form of the topological edge state by delocalizing them.[39–41] The reciprocity is usually broken with different real parts of the coupling depending on the direction of propagation, which corresponds to amplification in one direction of propagation and a decrease in the other. Alternatively, the reciprocity of the wave propagation can be broken by considering imaginary parts in the coupling, which involves that the couplings induce a phase shift that depends on the direction of propagation. This corresponds to phase non-reciprocity, which has been much less explored.[42]

In this work, we consider a one-dimensional acoustic SSH model with nonreciprocal couplings where the non-reciprocity is introduced in the imaginary parts of the couplings. The imaginary parts of the couplings, by acting on the magnitude of the coupling, can induce the dimerization of the SSH chain, which can lead to a topological phase transition. Three types of configurations can be obtained in this system. This system can be non-reciprocal and non-Hermitian, non-reciprocal but Hermitian, and, finally, non-Hermitian but reciprocal.

This work is organized as follows. We start in Sec. II by describing the acoustic SSH model and the tight-binding model that is considered to describe it. Then, the topological properties of the Hermitian case are specifically studied before generalizing to the non-Hermitian case. In Sec. III, the Hermitian acoustic SSH is modeled with the transfer matrix method. The phase non-reciprocity is induced by a mean air flow in one of the couplings of the unit cells. The band structures are then derived by considering the acoustic SSH chain as nonreciprocal Willis materials.[43–45] The topological edge states are then exposed with finite element numerical simulations.

II. TOPOLOGY OF THE SSH MODEL WITH NON-RECIPROCAL COUPLINGS

The acoustic SSH unit cell is composed of two sites A and B with resonant cylindrical cavities of length $L_{res} = 8$ cm and radius $R_{res} = 1.6$ cm connected by tubes of length $L_{co} = 7$ cm and radius $R_{co} = 0.8$ cm as shown in Fig. 1. The length of the unit cell is $a = 2L_{res} + 2L_{co}$. The resonators have a dipolar resonance at $f_0 = 4027$ Hz. The tubes induce a real coupling strength $t_0 = 120$ Hz. Going beyond the standard model, the reciprocity of wave propagation in one of the connecting tubes is broken by adding imaginary parts it_1 in the backward direction and it_2 in the forward direction, which corresponds to phase non-reciprocity. Here, the parameters f_0, t_0, t_0', t_1, and t_2 are kept real. We consider two unit cells: U_1 and U_2. In the first unit cell U_1, the intracell connection is non-reciprocal while keeping a reciprocal intercell connection as shown in Fig. 1(b) and where the Bloch Hamiltonian is written using a tight-binding model,

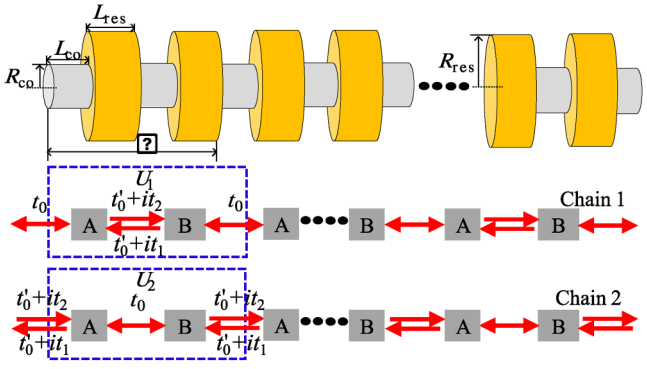

FIG. 1. Schematics of the acoustic SSH chain with the unit cell U_1 and the unit cell U_2.

$$H_1 = \begin{bmatrix} f_0 & \left(t_0' + it_1\right) + t_0 e^{-iqa} \\ \left(t_0' + it_2\right) + t_0 e^{iqa} & f_0 \end{bmatrix}, \quad (1)$$

where q is the Bloch wavenumber. The chiral symmetry with respect to the resonant frequency f_0 induces the quantization of the non-Hermitian Zak phase.[46] $t_0 = t_0'$ when the internal radii of the coupling waveguides are equal, and $t_0 \neq t_0'$, otherwise. In the second unit cell U_2, the intercell connection is non-reciprocal while keeping a reciprocal intracell connection as shown in Fig. 1(b) and where the Bloch Hamiltonian is written as

$$H_2 = \begin{bmatrix} f_0 & t_0 + \left(t_0' + it_1\right) e^{-iqa} \\ t_0 + \left(t_0' + it_2\right) e^{iqa} & f_0 \end{bmatrix}. \quad (2)$$

Finite chains with an open boundary condition on each end composed of N unit cells U_1 are described by the Hamiltonian,

$$\begin{aligned} H_{O1} = {} & \left(t_0' + it_1\right)\left[\sum_{n=1}^{N} c_{A,n}^{\dagger} c_{B,n}\right] + \left(t_0' + it_2\right)\left[\sum_{n=1}^{N} c_{B,n}^{\dagger} c_{A,n}\right] \\ & + t_0\left[\sum_{n=1}^{N-1} c_{A,n+1}^{\dagger} c_{B,n} + c_{B,n}^{\dagger} c_{A,n+1}\right] \\ & + f_0\left[\sum_{n=1}^{N} c_{A,n}^{\dagger} c_{A,n} + c_{B,n}^{\dagger} c_{B,n}\right], \end{aligned} \quad (3)$$

where $c_{A,n}$ and $c_{A,n}^{\dagger}$ are the creation and annihilation operators of site A, respectively, and for the chain composed of unit cells U_2, the Hamiltonian is written as

$$\begin{aligned} H_{O2} = {} & t_0\left[\sum_{n=1}^{N} c_{A,n}^{\dagger} c_{B,n} + c_{B,n}^{\dagger} c_{A,n}\right] + \left(t_0' + it_1\right)\left[\sum_{n=1}^{N-1} c_{B,n}^{\dagger} c_{A,n+1}\right] \\ & + \left(t_0' + it_2\right)\left[\sum_{n=1}^{N-1} c_{A,n+1}^{\dagger} c_{B,n}\right] + f_0\left[\sum_{n=1}^{N} c_{A,n}^{\dagger} c_{A,n} + c_{B,n}^{\dagger} c_{B,n}\right]. \end{aligned} \quad (4)$$

In this work, the finite chains with open boundaries are composed of 15 unit cells. Before analyzing the general non-Hermitian case, we first consider a special case, which is Hermitian.

A. Hermitian case

The model in Eqs. (1) and (2) becomes Hermitian when $t_2 = -t_1$, and the eigenvalues of the Hamiltonian H_1 read

$$E_{1,2} = f_0 \pm \left[t_0^2 + \left(t_0' + it_1\right)\left(t_0' - it_1\right) + t_0\left(t_0' + it_1\right)e^{iqa} + t_0\left(t_0' - it_1\right)e^{-iqa}\right]^{\frac{1}{2}} = f_0 \pm \left[t_0^2 + tt^\dagger + t_0 t^\dagger e^{iqa} + t_0 t e^{-iqa}\right]^{\frac{1}{2}}, \quad (5)$$

with $t = t_0' + it_1$, and the eigenvalues of H_2 read

$$E_{1,2} = f_0 \pm \left[t_0^2 + tt^\dagger + t_0 t e^{iqa} + t_0 t^\dagger e^{-iqa}\right]^{\frac{1}{2}}. \quad (6)$$

The Dirac point is located at the Brillouin zone boundary only if $t_1 = 0$ Hz, as shown in Fig. 2(a). As a result of the non-reciprocity when $t_1 \neq 0$ giving $\mathrm{Im}(t) \neq 0$, the bands are not symmetric anymore with respect to $q = 0$. With $|t| = t_0$, the Dirac point is visible away from the Brillouin zone boundary as shown in Fig. 2(b). The Dirac degeneracy is lifted when $|t| \neq t_0$, as shown in Fig. 2(c). This denotes that a topological phase transition occurs when $|t| = t_0$. Since the model is Hermitian, the topological phase can be characterized by the Zak phase,

$$Z = \frac{i}{2\pi}\int_q \langle \mathbf{u}_n | \partial_q \mathbf{u}_n \rangle dq, \quad (7)$$

where $\mathbf{u}_n$ is the eigenvector of the band n. The dependence of the Zak phases of the two unit cells U_1 and U_2 as a function of t_0' and t_1 is shown in Figs. 2(e) and 2(f). One can see that the cell is topologically trivial when the magnitude of the intracell coupling is smaller than the one of the intercell couplings, while being topologically nontrivial otherwise. In the case where the intracell and intercell couplings have the same radius giving $t_0' = t_0$, the unit cell U_1 is trivial and the unit cell U_2 is nontrivial if $t_1 \neq 0$. Using Eqs. (3) or (4), the eigenfrequencies of finite chains with open boundaries exhibit two topological edge states in the nontrivial case, while no edge state is visible when the finite chain is composed of a trivial unit as shown in Fig. 2(d). The mode shape of the topological edge state is shown in Fig. 2(g). An acoustic implementation of this Hermitian case with the transfer matrix method is shown in Sec. III.

B. General non-Hermitian case

In the case where $t_2 \neq -t_1$, the model is non-Hermitian with complex eigenfrequencies and where the conventional BBC is broken as expected for a non-Hermitian SSH model with non-reciprocal couplings.[2,4,46,47] Taking the case of couplings having equal real parts, i.e., $t_0' = t_0$ and under a Periodic Boundary Condition (PBC), the gap between the two bands given by the complex eigenfrequencies of Eqs. (1) and (2) closes when either $t_1 = 0$ or $t_2 = 0$ at $q = \pm\pi/a$. This is in contradiction when the Open Boundary Condition (OBC) is considered where the gap is still opened when either $t_1 = 0$ or $t_2 = 0$. This inequivalence between PBC and OBC is stemming from the non-Bloch wave nature of the eigenstates due to the non-Hermitian skin effect (NHSE).[4] The BBC can be re-established following the non-Bloch approach in the generalized Brillouin zone using the similarity

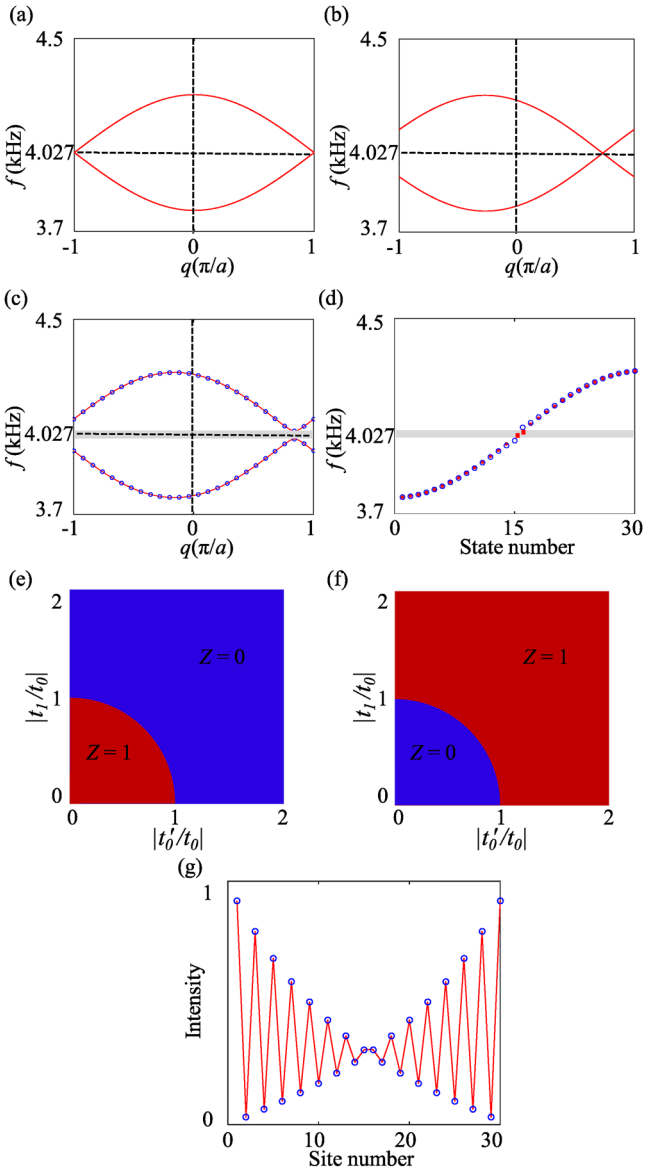

FIG. 2. Band structures of the SSH model (a) with no phase non-reciprocity, $t_0 = t_0' = 120$ Hz and $t_1 = 0$ Hz; (b) with phase non-reciprocity and the Dirac degeneracy still closed $t_0 = 120$ Hz, $t_0' = 70$ Hz, and $t_1 = -\sqrt{120^2 - 70^2}$ Hz; (c) with phase non-reciprocity and a frequency bandgap, $t_0 = t_0' = 120$ Hz and $t_1 = -70$ Hz for the unit cell U_1 (blue dots) and the unit cell U_2 (red curve). (d) Eigenfrequencies of finite chains with open boundaries composed of 15 unit cells U_1 (blue circles) and U_2 (red stars) with the same parameters as in (c). Two topological edge states are visible in the bandgap when the finite chain is composed of the cell U_2. A topological phase diagram of the unit cells (e) U_1 and (f) U_2. (g) Mode shape of the topological edge state with the same parameters as in (c).

transformation of the Hamiltonians $H_{O1,2}$,[4]

$$\bar{H}_{O1,2} = S^{-1} H_{O1,2} S, \tag{8}$$

where S is a diagonal matrix whose diagonal elements are $\{r, r, r^2, r^2, \ldots, r^N, r^N\}$ and $\{1, r, r, r^2, r^2, \ldots, r^{N-1}, r^N\}$ when the similarity transformation is applied to H_{O1} and H_{O2}, respectively. Taking the case where $r = \sqrt{(t_0' + it_1)/(t_0' + it_2)}$, $\bar{H}_{O1,2}$ are still non-Hermitian in general but become reciprocal; thus, it annihilates the NHSE. The different couplings are transformed as follows:

$$\begin{aligned} t_0 \Rightarrow t_0,\ (t_0' + it_1) \Rightarrow \bar{t}_1 = \sqrt{(t_0' + it_1)(t_0' + it_2)}, \\ \text{and}\ \ (t_0' + it_2) \Rightarrow \bar{t}_1 = \sqrt{(t_0' + it_1)(t_0' + it_2)}. \end{aligned} \tag{9}$$

Since the NHSE is annihilated, the BBC is restored and the associated bulk Hamiltonians can then be written as

$$\bar{H}_1 = \begin{bmatrix} f_0 & \bar{t}_1 + t_0 e^{-iqa} \\ \bar{t}_1 + t_0 e^{iqa} & f_0 \end{bmatrix} \tag{10}$$

and

$$\bar{H}_2 = \begin{bmatrix} f_0 & t_0 + \bar{t}_1 e^{-iqa} \\ t_0 + \bar{t}_1 e^{iqa} & f_0 \end{bmatrix}. \tag{11}$$

The conditions for gap closing and a topological phase transition can then be generalized to the non-Hermitian case with $t_0 = |\sqrt{(t_0' + it_1)(t_0' + it_2)}|$. The unit cell U_1 is non-trivial when $t_0 > |\sqrt{(t_0' + it_1)(t_0' + it_2)}|$ and is trivial otherwise as shown in Fig. 3(a) where the topological edge states are visible in the non-trivial phase. Conversely, the unit cell U_2 is non-trivial when $t_0 < |\sqrt{(t_0' + it_1)(t_0' + it_2)}|$ and is trivial otherwise as shown in Fig. 3(b).

In the general non-Hermitian case, the field localization under OBC is importantly influenced by the NHSE. The eigenfrequencies of the bulk Hamiltonians in Eqs. (1) and (2) form closed loops in the complex frequency plane. The winding direction of the loop is characterized by the spectral winding number with respect to a reference frequency f_r,[39]

$$w(f_r) = \frac{1}{2\pi} \oint_{BZ} \frac{d}{dq} \arg \det [H_{1,2}(q) - f_r] dq. \tag{12}$$

The spectral winding number $w(f_r)$ is +1 (−1) if the winding direction is anti-clockwise (clockwise) around the reference frequency f_r, respectively, and is 0 in the absence of NHSE.[29,48,49] A spectral winding number of +1 (−1) indicates that the eigenstates localize on the right (left) side of the open chain, respectively. The phase diagram of the spectral winding number in our system is shown in Fig. 4(a). When $|t_1| < |t_2|$, the winding direction is anti-clockwise with $w(f_r) = 1$ and the eigenstates localize on the right-hand side of the open chain as shown in Fig. 4(c). It should be noticed that the NHSE can compete with the localization of the topological

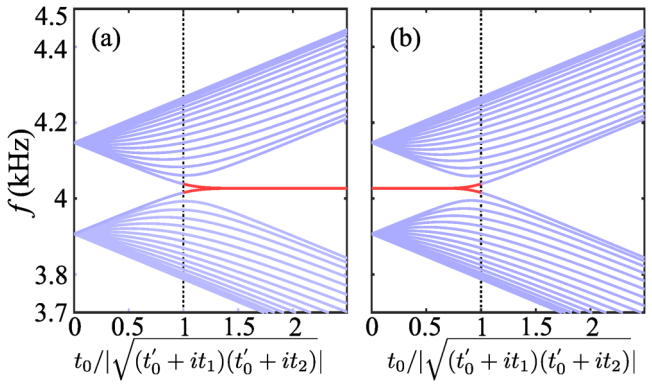

FIG. 3. Eigenfrequencies of the finite chain under OBC (a) composed of the unit cell U_1 and (b) composed of the unit cell U_2.

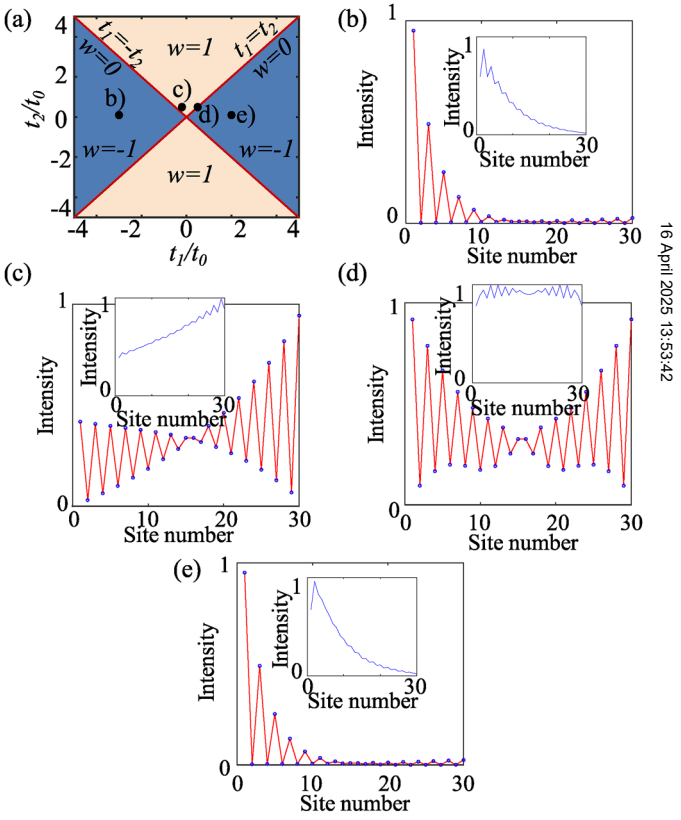

FIG. 4. Skin effect in a chain composed of unit cells U_2 with $t_0 = t_0' = 120$ Hz. (a) Phase diagram of the spectral winding number w of the Bloch Hamiltonian H_2. A mode shape of the topological edge states in a finite chain under OBC composed of 15 unit cells U_2 with (b) $t_1 = -300$ Hz and $t_2 = 10$ Hz, (c) $t_1 = 20$ Hz and $t_2 = 50$ Hz, (d) $t_1 = 50$ Hz and $t_2 = 50$ Hz, and (e) $t_1 = 200$ Hz and $t_2 = 10$ Hz. The insets in (b)–(e) show the mode shape of the bulk eigenmodes.

edge states.[39–41] Two transition points occur where the eigenfrequencies form only one-dimensional lines instead of the closed loop and the spectral winding number is zero. The first one is found when the system is Hermitian, i.e., $t_1 = -t_2$, which corresponds to the case in Fig. 2. Thus, the imaginary components of the eigenfrequencies are vanishing and the eigenfrequencies are one-dimensional lines in the complex frequency plane. The second one is found when the system is reciprocal but still non-Hermitian, i.e., $t_1 = t_2$, as shown in Fig. 4(d). When $|t_1| > |t_2|$, the winding direction in clockwise; thus, the spectral winding number is -1 and the eigenstates localize to the left of the chain as shown in Figs. 4(b) and 4(e).

III. ACOUSTIC MODEL OF THE HERMITIAN SSH WITH NONRECIPROCAL COUPLINGS

In this section, we describe the acoustic implementation that corresponds to the tight-binding model. Assuming the one-dimensional character of the acoustic wave propagation in the waveguides, the acoustic field at one point of the chain is given by the state vector $\mathbf{W}^T = [P, U]$, where P is the acoustic pressure, U is the acoustic velocity, and T is the transpose operator. The state vector at the right end of a cell of length d is deduced from the state vector at the left end of the cell via the transfer matrix $\mathbf{T}$,

$$\mathbf{W}(d) = \mathbf{T}\mathbf{W}(0). \tag{13}$$

The total transfer matrix of a cell is found by multiplying the transfer matrices of each individual element that compose it. Here, the transfer matrix of a waveguide $\mathbf{T}_w$ of radius R and length L is given by

$$\mathbf{T}_w = \begin{pmatrix} \cos(kL) & iZ_c\sin(kL) \\ i\sin(kL)/Z_c & \cos(kL) \end{pmatrix}, \tag{14}$$

where the time convention is $e^{-i\omega t}$ and $Z_c = \rho_0 c_0/S$ is the characteristic impedance of the waveguide, where $S = \pi R^2$, ρ_0 is the air mass density, and c_0 is the sound velocity. The transfer matrices $\mathbf{T}_{\text{res}}$ and $\mathbf{T}^{\text{r}}_{\text{co}}$ of the resonators and the reciprocal couplings, respectively, are found using Eq. (14) by applying the corresponding dimensions, i.e., R_{res}, R_{co}, and L_{co}. A correction length, which comes from radiation at the change of section in the waveguide, is added to the length of the resonator, i.e., $L^{\text{TMM}}_{\text{res}} = L_{\text{res}} + 0.2$ cm to fit with the numerical results. When a mean air flow is introduced in a waveguide, the acoustic wave propagation becomes phase non-reciprocal. Neglecting the flow-acoustic instabilities, the transfer matrix is then written as[50]

$$\mathbf{T}^{\text{nr}}_{\text{co}} = e^{-ik_f ML}\begin{pmatrix} \cos(k_f L) & iZ_c\sin(k_f L) \\ i\sin(k_f L)/Z_c & \cos(k_f L) \end{pmatrix}, \tag{15}$$

where $k_f = k/(1 - M^2)$ is the convective wavenumber and M is the Mach number of the mean air flow. To implement in an experimental setup, the air flow needs to be restricted to the waveguide taking the role of the coupling. To this end, one can follow the setup proposed in Ref. 51, where a pipe, which contains a fan, is connected to both ends of the coupling. Acoustic impedance mismatch, using Helmholtz resonators for instance, on both ends of the pipe ensures that the acoustic waves travel only through the waveguide. Combining Eqs. (14) and (15), the transfer matrices $\mathbf{T}_1$ and $\mathbf{T}_2$ of the unit cells U_1 and U_2 can be build with

$$\mathbf{T}_1 = \mathbf{T}^{\text{r}}_{\text{co}}\mathbf{T}_{\text{res}}\mathbf{T}^{nr}_{co}\mathbf{T}_{\text{res}}\mathbf{T}^{\text{r}}_{\text{co}} \text{ and} \tag{16}$$

$$\mathbf{T}_2 = \mathbf{T}^{\text{nr}}_{\text{co}}\mathbf{T}_{\text{res}}\mathbf{T}^{\text{r}}_{\text{co}}\mathbf{T}_{\text{res}}\mathbf{T}^{nr}_{\text{co}}, \tag{17}$$

respectively. To ensure that the unit cells have the correct length, the transfer matrices of the couplings on both ends of the unit cells, i.e., $\mathbf{T}^{\text{r}}_{\text{co}}$ ($\mathbf{T}^{\text{nr}}_{\text{co}}$) for the cell U_1 (U_2), respectively, are derived using half of the length of the intercell coupling. The transmission coefficients of the scattering matrix for left t_L and right t_R incidence are deduced from the inverse of the total transfer matrix with

$$\mathbf{T}^{-1} = \begin{pmatrix} A & B \\ C & D \end{pmatrix}, \tag{18}$$

with

$$\begin{aligned} t_L &= \frac{2}{A + B/Z_c + Z_c C + D}, \\ t_R &= \frac{2(AD - BC)}{A + B/Z_c + Z_c C + D}, \end{aligned} \tag{19}$$

where the characteristic impedance Z_c is one of the intercell couplings. The transmission coefficients through a chain composed of 15 unit cells have equal amplitudes between the reciprocal case with no mean flow with $M = 0$ and the non-reciprocal case with a mean flow in one of the couplings with $M = 0.15$ as shown in Figs. 5(a) and 5(c). Furthermore, the amplitudes are equal for left and right incidence, confirming that the non-reciprocity induced by the mean flow does not affect the amplitude as shown in Figs. 5(a) and 5(c). The amplitudes are equal to one between 3.8 and 4.3 kHz. The unity transmission corresponds to the frequency range of the two modes predicted by the tight-binding model. In the non-reciprocal case, the tight-binding model predicts the existence of a bandgap, which is visible in Fig. 5(c) around 4 kHz. The mean flow induces a phase non-reciprocity as can be seen in Fig. 5(d) where the phases of the transmission coefficients differ for left and right incidences, contrary to the reciprocal case where the phase of the transmission coefficients is equal between left and right incidences.

Stemming from the mass and momentum conservation laws, the acoustic state vector $\mathbf{W}$ satisfies[43–45]

$$\frac{d}{dx}\mathbf{W} = \mathbf{A}\mathbf{W}, \tag{20}$$

where the matrix $\mathbf{A}$ is written for non-reciprocal Willis materials as

$$\mathbf{A} = i\omega\begin{pmatrix} \chi_e + \chi_{nr} & \rho_e \\ C_e & -\chi_e + \chi_{nr} \end{pmatrix}, \tag{21}$$

where ρ_e is the effective density, C_e is the effective compressibility, χ_e is the even Willis coupling, and χ_{nr} is the nonreciprocal Willis coupling. It follows from Eq. (21) that for a cell of length d,

$$\mathbf{W}(d) = e^{\mathbf{A}d}\mathbf{W}(0). \tag{22}$$

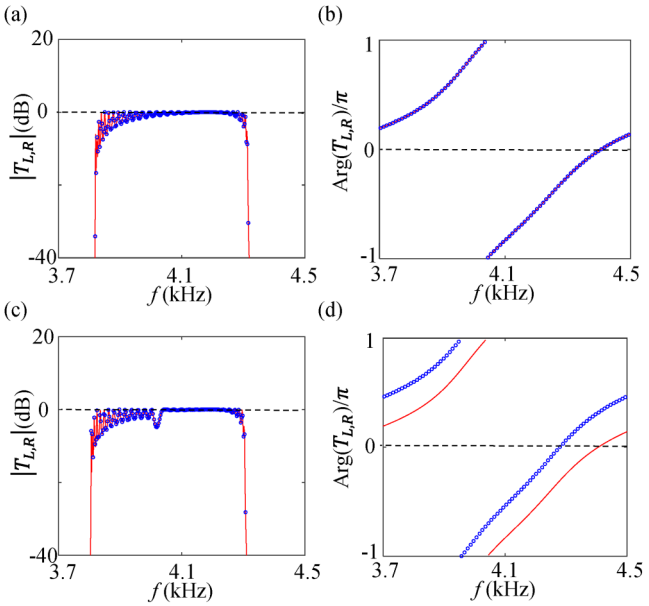

FIG. 5. Amplitudes of the transmission coefficients under left incidence (red curve) and right incidence (blue circles) of a chain composed of 15 unit cells with (a) $M = 0$ and (c) $M = 0.15$. Phases of the transmission coefficients under left incidence (red curve) and right incidence (blue circles) of one unit cell with (b) $M = 0$ and (d) $M = 0.15$.

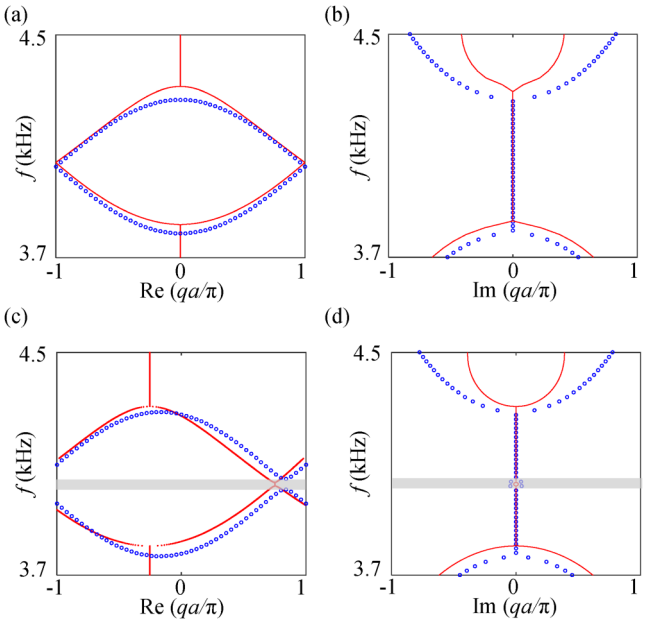

FIG. 6. Band structures of the SSH unit cells derived with the transfer matrix method (blue circle) compared to the tight binding method (red curves). (a) and (c) Real parts of the wavenumbers. (b) and (d) Imaginary parts of the real number. (a) and (b) $M = 0$. (c) and (d) $M = 0.15$. The gray area denotes the bandgap.

By comparing Eqs. (13) and (22), the matrix exponential of $\mathbf{A}d$ identifies with the transfer matrix $\mathbf{T}$. Therefore, the dispersion relations of the acoustic wave propagating in the periodic non-reciprocal acoustic SSH model can be retrieved by calculating the wave numbers using the Willis parameters with[52]

$$k_{\pm} = -\omega\chi_{nr} \pm \omega\sqrt{-|\chi_e|^2 + \rho_e C_e}. \tag{23}$$

The wave numbers calculated with Eq. (23) are in good agreement with the eigenfrequencies of the Hermitian tight-binding model in Eqs. (5) and (6) as shown in Fig. 6. The additional mean flow in one of the couplings breaks the reciprocity of the wave propagation and opens the bandgap as can be seen in Figs. 6(c) and 6(d).

To further explore the topological properties of the acoustic SSH model, we construct a finite element model composed of 15 unit cells with open boundaries. An acoustic wave is excited at one of the open boundaries, and the amplitude of the acoustic pressure at that boundary is measured by positioning both the source and the receiver in the resonator at the boundary. A mean air flow is introduced in the corresponding coupling tubes. As can be seen in Fig. 7(a) where the acoustic amplitude drops in the frequency bandgap when the finite chain is composed of unit cells in the topological trivial phase. When the finite chain is composed of unit cells in the non-trivial topological phase, a peak in the acoustic amplitude denotes the presence of the topological edge state. Furthermore, this topological edge state is observed on both ends of the finite chain as shown in Fig. 7(b).

These results confirm that the phase non-reciprocal SSH can be realized experimentally and that the acoustic implementation provides a convenient platform to emulate the results found in

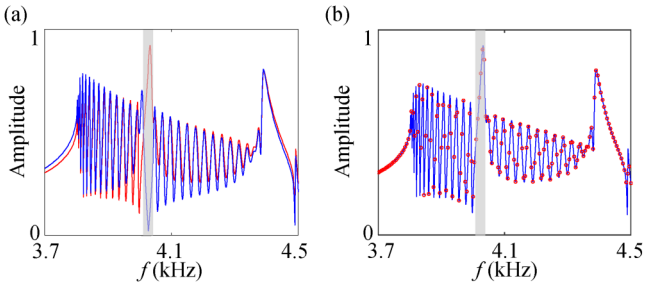

FIG. 7. Acoustic response of the acoustic SSH chain at the open boundaries from the finite element numerical calculations. (a) Amplitude of the acoustic pressure at the left open boundary when the wave excited that boundary. The SSH chain is composed of unit cells U_1 in the trivial phase (blue curve) and of unit cells U_2 in the nontrivial phase (red curve). The peak of amplitude of the red curve in the gray area corresponds to the topological edge state. (b) Amplitude of the edge state at the left (red dots) and right (blue curve) open boundaries.

Sec. II A. The general non-Hermitian case with phase non-reciprocity is more delicate to realize in a real model, but it might be implemented using the non-reciprocal control of the phase in Janus acoustic metamaterials.[53] In Ref. 53, the phase shift in an acoustic waveguide is nonreciprocal and independently controlled for the two different directions of wave propagation using two three-port acoustic circulators.

IV. CONCLUSION

To summarize, we have shown that the introduction of phase non-reciprocity in the coupling can induce the dimerization to build an SSH chain. The phase non-reciprocity is modeled in a tight-binding model by adding imaginary parts to the couplings between sites. When the imaginary parts are opposite between the two directions of propagation, the model remains Hermitian. The bands are not symmetric anymore around the center of the Brillouin zone, and the bandgap can be opened because the magnitudes of the couplings differ, hence the dimerization. Topological non-trivial phases are found, and the topological edge states are visible at the open boundaries. This Hermitian SSH chain can be mimicked in an acoustic model by introducing a mean air flow in one of the couplings, which induce the phase non-reciprocity between the two directions of propagation. When the values of the imaginary parts of the coupling are not opposite, the model becomes non-Hermitian. The chain experiences the non-Hermitian skin effect, and the conventional bulk boundary correspondence is broken, which can be reestablished through the non-Bloch approach that allows us to describe the different topological phases of the chain. When the imaginary parts of the coupling are equal (but different from zero), the model remains non-Hermitian but becomes reciprocal, which annihilates the non-Hermitian skin effect. The direction of the skin effect depends on the ratio of the two imaginary parts with the two transition points where it is annihilated: the Hermitian case and the reciprocal case.

AUTHOR DECLARATIONS

Conflict of Interest

The authors have no conflicts to disclose.

Author Contributions

Tong Guo: Formal analysis (equal); Investigation (equal); Methodology (equal); Software (equal); Visualization (equal); Writing – original draft (equal); Writing – review & editing (equal). **Liyun Cao:** Supervision (equal); Validation (equal); Writing – original draft (equal); Writing – review & editing (equal). **Badreddine Assouar:** Validation (equal); Writing – original draft (equal); Writing – review & editing (equal). **Brice Vincent:** Formal analysis (equal); Investigation (equal); Methodology (equal); Software (equal); Supervision (equal); Validation (equal); Visualization (equal); Writing – original draft (equal); Writing – review & editing (equal). **Aurélien Merkel:** Conceptualization (equal); Formal analysis (equal); Investigation (equal); Methodology (equal); Software (equal); Supervision (equal); Validation (equal); Visualization (equal); Writing – original draft (equal); Writing – review & editing (equal).

DATA AVAILABILITY

The data that support the findings of this study are available from the corresponding author upon reasonable request.

REFERENCES

[1]T. E. Lee, "Anomalous edge states in a non-Hermitian lattice," Phys. Rev. Lett. **116**, 133903 (2016).
[2]Y. Xiong, "Why does bulk boundary correspondence fail in some non-Hermitian topological models," J. Phys. Commun. **2**, 035043 (2018).
[3]J. Cheng, X. Zhang, M.-H. Lu, and Y.-F. Chen, "Competition between band topology and non-hermiticity," Phys. Rev. B **105**, 094103 (2022).
[4]S. Yao and Z. Wang, "Edge states and topological invariants of non-Hermitian systems," Phys. Rev. Lett. **121**, 086803 (2018).
[5]L. E. F. Foa Torres, "Perspective on topological states of non-Hermitian lattices," J. Phys. Mater. **3**, 014002 (2020).
[6]Y. Z. Han, J. S. Liu, and C. S. Liu, "The topological counterparts of non-Hermitian SSH models," New J. Phys. **23**, 123029 (2021).
[7]E. J. Bergholtz, J. C. Budich, and F. K. Kunst, "Exceptional topology in non-Hermitian systems," Rev. Mod. Phys. **93**, 015005 (2021).
[8]K. Ding, C. Fang, and G. Ma, "Non-Hermitian topology and exceptional-point geometries," Nat. Rev. Phys. **4**, 745 (2022).
[9]H. Schomerus, "Topologically protected midgap states in complex photonic lattices," Opt. Lett. **38**, 1912–1914 (2013).
[10]C. Poli, M. Bellec, U. Kuhl, F. Mortessagne, and H. Schomerus, "Selective enhancement of topologically induced interface states in a dielectric resonator chain," Nat. Commun. **6**, 6710 (2015).
[11]J. M. Zeuner, M. C. Rechtsman, Y. Plotnik, Y. Lumer, S. Nolte, M. S. Rudner, M. Segev, and A. Szameit, "Observation of a topological transition in the bulk of a non-Hermitian system," Phys. Rev. Lett. **115**, 040402 (2015).
[12]S. Weimann, M. Kremer, Y. Plotnik, Y. Lumer, S. Nolte, K. G. Makris, M. Segev, M. C. Rechtsman, and A. Szameit, "Topologically protected bound states in photonic parity–time-symmetric crystals," Nat. Mater. **16**, 433–438 (2017).
[13]B. Hu, Z. Zhang, H. Zhang, L. Zheng, W. Xiong, Z. Yue, X. Wang, J. Xu, Y. Cheng, X. Liu, and J. Christensen, "Non-Hermitian topological whispering gallery," Nature **597**, 655–659 (2021).
[14]A. F. Tzortzakakis, A. Katsaris, N. E. Palaiodimopoulos, P. A. Kalozoumis, G. Theocharis, F. K. Diakonos, and D. Petrosyan, "Topological edge states of the PT-symmetric Su-Schrieffer-Heeger model: An effective two-state description," Phys. Rev. A **106**, 023513 (2022).
[15]Z. Zhang, M. Rosendo López, Y. Chen, X. Liu, and J. Christensen, "Non-Hermitian sonic second order topological insulator," Phys. Rev. Lett. **122**, 195501 (2019).
[16]H. Zhao, P. Miao, M. H. Teimourpour, S. Malzard, R. El-Ganainy, H. Schomerus, and L. Feng, "Topological hybrid silicon microlasers and," Nat. Commun. **9**, 981 (2018).
[17]S. Malzard, C. Poli, and H. Schomerus, "Topologically protected defect states in open photonic systems with non-Hermitian charge-conjugation and parity-time symmetry," Phys. Rev. Lett. **115**, 200402 (2015).
[18]K. Takata and M. Notomi, "Photonic topological insulating phase induced solely by gain and loss," Phys. Rev. Lett. **121**, 213902 (2018).
[19]X.-W. Luo and C. Zhang, "Higher-order topological corner states induced by gain and loss," Phys. Rev. Lett. **123**, 073601 (2019).
[20]H. Gao, H. Xue, Q. Wang, Z. Gu, T. Liu, J. Zhu, and B. Zhang, "Observation of topological edge states induced solely by non-hermiticity in an acoustic crystal," Phys. Rev. B **101**, 180303 (2020).
[21]S. Liu, S. Ma, C. Yang, L. Zhang, W. Gao, Y. J. Xiang, T. J. Cui, and S. Zhang, "Gain- and loss-induced topological insulating phase in a non-Hermitian electrical circuit," Phys. Rev. Appl. **13**, 014047 (2020).

[22]H. Gao, H. Xue, Q. Wang, Z. Gu, T. Liu, J. Zhu, and B. Zhang, "Non-Hermitian route to higher-order topology in an acoustic crystal," Nat. Commun. **12**, 1888 (2021).
[23]H. Fan, H. Gao, S. An, Z. Gu, S. Liang, Y. Zheng, and T. Liu, "Hermitian and non-Hermitian topological edge states in one-dimensional perturbative elastic metamaterials," Mech. Syst. Signal Process. **169**, 108774 (2022).
[24]H. Fan, H. Gao, S. An, Z. Gu, Y. Chen, S. Huang, S. Liang, J. Zhu, T. Liu, and Z. Su, "Observation of non-hermiticity-induced topological edge states in the continuum in a trimerized elastic lattice," Phys. Rev. B **106**, L180302 (2022).
[25]H. Li, C. Luo, T. Zhang, X. Zhou, J. Xu, J. Xu, S. Duan, X. Deng, and Y. Shen, "Non-Hermitian total-loss high-order topological insulator based on 1d Su–Schrieffer–Heeger (SSH)," Physica B **650**, 414570 (2023).
[26]H. Wetter, M. Fleischhauer, S. Linden, and J. Schmitt, "Observation of topological edge state stabilized by dissipation," Phys. Rev. Lett. **131**, 083801 (2023).
[27]T. Guo, B. Assouar, B. Vincent, and A. Merkel, "Edge states in non-Hermitian composite acoustic Su Schrieffer Heeger chains," J. Appl. Phys. **135**, 043102 (2024).
[28]X. Zhang, T. Zhang, M.-H. Lu, and Y.-F. Chen, "A review on non-Hermitian skin effect," Adv. Phys. X **7**, 2109431 (2022).
[29]R. Lin, T. Tai, L. Li, and C. H. Lee, "Topological non-Hermitian skin effect," Front. Phys. **18**, 53605 (2023).
[30]M. Brandenbourger, X. Locsin, E. Lerner, and C. Coulais, "Non-reciprocal robotic metamaterials," Nat. Commun. **10**, 4608 (2019).
[31]A. Ghatak, M. Brandenbourger, J. van Wezel, and C. Coulais, "Observation of non-Hermitian topology and its bulk–edge correspondence in an active mechanical metamaterial," Proc. Natl. Acad. Sci. U.S.A. **117**, 29561–29568 (2020).
[32]S. Weidemann, M. Kremer, T. Helbig, T. Hofmann, A. Stegmaier, M. Greiter, R. Thomale, and A. Szameit, "Topological funneling of light," Science **368**, 311–314 (2020).
[33]Y. Chen, X. Li, C. Scheibner, V. Vitelli, and G. Huang, "Realization of active metamaterials with odd micropolar elasticity," Nat. Commun. **12**, 5935 (2021).
[34]L. Zhang, Y. Yang, Y. Ge, Y.-J. Guan, Q. Chen, Q. Yan, F. Chen, R. Xi, Y. Li, D. Jia, S.-Q. Yuan, H.-X. Sun, H. Chen, and B. Zhang, "Acoustic non-Hermitian skin effect from twisted winding topology," Nat. Commun. **12**, 6297 (2021).
[35]Z. Gu, H. Gao, H. Xue, J. Li, Z. Su, and J. Zhu, "Transient non-Hermitian skin effect," Nat. Commun. **13**, 7668 (2022).
[36]A. Maddi, Y. Auregan, G. Penelet, V. Pagneux, and V. Achilleos, "Exact analog of the Hatano-Nelson model in one-dimensional continuous nonreciprocal systems," Phys. Rev. Res. **6**, L012061 (2024).
[37]T. Helbig, T. Hofmann, S. Imhof, M. Abdelghany, A. Szameit, M. Greiter, and R. Thomale, "Generalized bulk–boundary correspondence in non-Hermitian topolectrical circuits," Nat. Phys. **16**, 747–750 (2020).
[38]S. Liu, R. Shao, S. Ma, L. Zhang, O. You, H. Wu, Y. J. Xiang, T. J. Cui, and S. Zhang, "Non-Hermitian skin effect in a non-Hermitian electrical circuit," Research **2021**, 5608038.
[39]W. Zhu, W. X. Teo, L. Li, and J. Gong, "Delocalization of topological edge states," Phys. Rev. B **103**, 195414 (2021).
[40]W. Wang, X. Wang, and G. Ma, "Non-Hermitian morphing of topological modes," Nature **608**, 50–55 (2022).
[41]X. Wang, W. Wang, and G. Ma, "Extended topological mode in a one-dimensional non-Hermitian acoustic crystal," AAPPS Bull. **33**, 23 (2023).
[42]V. Yannopapas, "Dirac points, topological edge modes and nonreciprocal transmission in one-dimensional metamaterial-based coupled cavity arrays," Int. J. Mod. Phys. B **28**, 1441006 (2014).
[43]A. Merkel, V. Romero-Garcìa, J.-P. Groby, J. Li, and J. Christensen, "Unidirectional zero sonic reflection in passive PT-symmetric Willis media," Phys. Rev. B **98**, 201102(R) (2018).
[44]J.-P. Groby, V. Romero-García, M. Malléjac, A. Merkel, V. Tournat, D. Torrent, and J. Li, "Analytical modeling of one-dimensional resonant asymmetric and reciprocal acoustic structures as Willis materials," New J. Phys. **23**, 053020 (2021).
[45]C. Olivier, G. Poignand, M. Malléjac, V. Romero-García, G. Penelet, A. Merkel, D. Torrent, J. Li, and J.-P. Groby, "Nonreciprocal and even Willis couplings in periodic thermoacoustic amplifiers," Phys. Rev. B **104**, 184109 (2021).
[46]C. Yin, H. Jiang, L. Li, R. Lü, and S. Chen, "Geometrical meaning of winding number and its characterization of topological phases in one-dimensional chiral non-Hermitian systems," Phys. Rev. A **97**, 052115 (2018).
[47]S. Lieu, "Topological phases in the non-Hermitian Su-Schrieffer-Heeger model," Phys. Rev. B **97**, 045106 (2018).
[48]K. Zhang, Z. Yang, and C. Fang, "Correspondence between winding numbers and skin modes in non-Hermitian systems," Phys. Rev. Lett. **125**, 126402 (2020).
[49]N. Okuma, K. Kawabata, K. Shiozaki, and M. Sato, "Topological origin of non-Hermitian skin effects," Phys. Rev. Lett. **124**, 086801 (2020).
[50]M. L. Munjal, "Velocity ratio-cum-transfer matrix method for the evaluation of a muffler with mean flow," J. Sound Vib. **39**, 105–119 (1975).
[51]L. Quan, D. L. Sounas, and A. Alú, "Nonreciprocal Willis coupling in zero-index moving media," Phys. Rev. Lett. **123**, 064301 (2019).
[52]C. F. Sieck, A. Alù, and M. R. Haberman, "Origins of Willis coupling and acoustic bianisotropy in acoustic metamaterials through source-driven homogenization," Phys. Rev. B **96**, 104303 (2017).
[53]Y. Zhu, L. Cao, A. Merkel, S.-W. Fan, B. Vincent, and B. Assouar, "Janus acoustic metascreen with nonreciprocal and reconfigurable phase modulations," Nat. Commun. **12**, 7089 (2021).